Determination of the Kinetic Parameters for the Crystallization of Paracetamol from Water Using Metastable Zone Width Experiments

Zoltan K. Nagy,*,† Mitsuko Fujiwara,‡ Xing Yi Woo,‡ and Richard D. Braatz‡

Loughborough University, Chemical Engineering Department, Loughborough, LE11 3TU, United Kingdom, and Department of Chemical and Biomolecular Engineering, University of Illinois at Urbana−Champaign, 600 South Mathews Avenue, Urbana, Illinois 61801

A new approach for the estimation of kinetic parameters of crystallization from data obtained during the determination of metastable zone width is presented. The method is based on a simplified dynamic model of the system, which combines the population balance and mass balance, as well as information provided by concentration and particle size distribution measurements using ATR-FTIR spectroscopy and laser backscattering to determine simultaneously the nucleation and growth parameters from the experimental data. The application of the proposed approach is illustrated for the cooling crystallization of paracetamol from water. The technique is compared to existing approaches for the determination of nucleation parameters from metastable zone width experiments and is used to corroborate the assumptions used in the classical approaches. The key conclusion is that the assumptions made in the existing approaches, which simplifies the parameters' estimation procedure, can result in substantial error in the nucleation kinetics.

1. Introduction

Crystallization from solution is an important purification process in the manufacturing of pharmaceuticals. Besides achieving the desired purity, the control of the crystal size distribution (CSD) of the pharmaceutical product is critical for efficient downstream operations and product effectiveness.[1−3] For batch cooling crystallization, the final CSD is determined by the supersaturation profile. Hence, the control of CSD involves designing an optimal model-based cooling trajectory to create the supersaturation profile required.[4−9] Such model-based control strategies and the resulting performance are strongly sensitive to the uncertainties of the model.[10,11] As a consequence, the development of a model that can adequately describe the process and the ability to accurately estimate the parameters in the model is of paramount importance.[4−7,10]

The final CSD in a batch crystallizer is determined by various kinetic processes, which include primary and secondary nucleation, crystal growth, aggregation, and breakage. Because a complete theoretical model for crystallization kinetics does not exist, primary nucleation and growth rates are usually expressed as empirical (or semiempirical) power-law equations with supersaturation as the independent variable.[12−14] The parameters of these expressions can be obtained by applying optimization techniques to fit the model predictions with experimental data.[8] In particular, estimating the parameters of the primary nucleation kinetics accurately has been a challenge, as it is impossible to detect the presence of nuclei, which are in the subnanometer range as soon as they are formed.

The primary nucleation kinetics can be estimated from measuring the metastable zone width for different cooling rates and solute concentrations.[12,15−17] The main advantage of these approaches is the simplicity of the experimental procedure. However, various assumptions are made to express the nucleation rate as a function of the measured variables (i.e., the metastable zone width and supersaturation rate) to estimate the parameters. Such assumptions could lead to inaccurate model parameters. In addition, the determination of the metastable limit varies with the detection methods used,[18] which can also increase the uncertainties of the estimated parameters.

As the nuclei have to grow to a detectable size at the metastable limit, both primary nucleation and growth kinetics should be simultaneously considered in the parameter estimation procedure. Besides measuring the metastable zone width, experimental information of the solution and solid phase obtained in situ during the crystallization process is required to estimate the nucleation and growth parameters within an acceptable level of uncertainty. This is now possible by the recent advances made in the process sensor technology.[19−24] Using such sensors, concentration measurements and particle size information can be collected during the experiments.

This article describes a more rigorous approach to *simultaneously* estimate the nucleation and growth kinetics from metastable zone experiments using a model of the crystallization process with dynamic population and mass balance equations. Experimental data obtained from in situ measurements of the solution concentration using ATR-FTIR spectroscopy[25−28] and in situ measurements of the particle size information using laser backscattering[29,30] are used to identify the parameters in the model. This approach is applied to the determination of the crystallization kinetics of paracetamol from water. The identified model is then used to assess the existing approaches for identifying nucleation kinetics from metastable zone width experiments.

Because the determination of the metastable zone is usually a necessary step for batch crystallization operation, the kinetic parameters can be obtained without additional experiments during the development of the batch crystallization process. However, the uncertainty in the estimated kinetic parameters in this proposed method is still relatively high. Therefore, this approach is proposed as a complement to the batch model identification technique,[8,24] for example, to serve as the initial kinetic parameters for iterative procedures used in parameter estimation.

* To whom correspondence should be addressed. Tel.: +44(0)1509 222516. E-mail: Z.K.Nagy@lboro.ac.uk.

† Loughborough University.

‡ University of Illinois at Urbana-Champaign.

10.1021/ie060637c CCC: $40.75
Published on Web 01/19/2008

2. Estimation of Nucleation Kinetics from Metastable Zone Experiments

The metastable zone is a region bounded by the solubility curve and the metastable limit, where the solution is supersaturated but spontaneous nucleation does not occur in sufficiently short time.[18] The metastable limit can be determined by the polythermal method,[12,18] in which the solution, slightly above its saturated temperature T_s, is cooled at a constant rate until crystals are detected. The induction time (t_{ind}) is defined as the period between the instant when the supersaturated state is generated and the time instant when the particles become detectable, with size L_d corresponding to the temperature T_{met}. In this section, three approaches for the determination of nucleation kinetics from metastable zone width experiments are presented. The first two methods are obtained from the existing literature, whereas the third method is a new approach based on a simplified but generic model of the crystallization systems, which captures simultaneously the effects of the nucleation and growth processes.

Method 1. In this classical approach, Nyvlt[12] considers a system where supersaturation is achieved by moderate cooling. It is assumed that the nucleation rate at the beginning of nucleation is equal to the supersaturation rate for a limited period of time during which the growth of the just formed crystals is neglected. The primary number nucleation rate is given as a function of maximum supersaturation ($\Delta C_{max} = C_{max} - C^*$) at the metastable limit,

$$B = k_b \Delta C_{max}^b \tag{1}$$

where k_b and b are the kinetic parameters, whereas the primary mass nucleation rate (B_m) used in Nyvlts's approach can be expressed as,

$$B_m = k_b k_v \rho_c L_d^{\,3} \Delta C_{max}^b = k_b' \Delta C_{max}^b \tag{2}$$

where k_b' is the kinetic parameter with respect to the mass nucleation rate, k_v is the volume shape factor, L_d is the size of the detectable nucleus, and ρ_c is the mass density of the crystal. The maximum supersaturation can be expressed in terms of the maximum undercooling (ΔT_{max}),

$$\Delta C_{max} = \left(\frac{dC^*}{dT}\right)\Delta T_{max} \tag{3}$$

where $C^*(T)$ is the equilibrium concentration of the solute. On the basis of the assumption that the nucleation rate is equal to the supersaturation rate,

$$B_m = \frac{dC^*}{dT}\beta \tag{4}$$

where $\beta = -dT/dt$ is the constant cooling rate. Combining eqs 2 and 4, the linear dependence of the maximum undercooling on the cooling rate is obtained for constant dC^*/dT.

$$\ln(\beta) = (b-1)\ln\left(\frac{dC^*}{dT}\right) + \ln(k_b') + b\ln(\Delta T_{max}) \tag{5}$$

From the measurements of metastable zone width at various cooling rates, it is possible to obtain the kinetic parameters for primary nucleation. Because growth of nuclei is not taken into account, this method gives the apparent nucleation parameter rather than the true parameter.[17]

Method 2. Without the presence of crystals, the formation of the solid phase is due to primary nucleation. Homogeneous nucleation occurs when sufficiently high supersaturation is reached, and heterogeneous nucleation occurs due to the presence of foreign particles at a lower supersaturation. Mersmann[13] expresses the rate of heterogeneous nucleation as

$$B = 0.965\varphi_{het} D_{AB}(N_A C_c)^{5/3}(C^*/C_c)^{7/3} S^{7/3}\sqrt{f\ln(C_c/C^*)} \times \exp\left(-1.19f\frac{(\ln(C_c/C^*))^3}{(\ln(S))^2}\right) \tag{6}$$

where φ_{het} is the heterogeneity factor, D_{AB} is the diffusion coefficient, C_c is the molar density of the crystal, N_A is the Avogadro number, f is the reduction factor, and $S = C/C^*$ is the supersaturation ratio. The values for f range from 0.1 to 1 and φ_{het} is approximately 10^{-11}. Equation 6 is also valid for homogeneous nucleation when $\varphi_{het} = 1$ and $f = 1$.

An approach to determine the kinetic parameters, φ_{het} and f, is proposed by Kim and Mersmann.[15] The induction time is written as a function of maximum undercooling (ΔT_{max}) or maximum supersaturation (ΔC_{max}), and constant cooling rate (β),

$$t_{ind} = \frac{\Delta T_{max}}{\beta} = \left(\frac{dC^*}{dT}\right)^{-1}\frac{\Delta C_{max}}{\beta} \tag{7}$$

It is further assumed that the supersaturation increases proportionally with the supersaturation rate during $t \le t_{ind}$, and the mass nucleation rate equals the supersaturation rate. Using the power-law relation in eq 1, the number of crystals formed spontaneously from $t = 0$ to t_{ind} can be expressed as

$$N = \frac{\Delta C_{max}}{(b+1)k_v C_c L_d^{\,3}} \tag{8}$$

The primary nucleation rate during $t \le t_{ind}$ is then approximated by

$$B = \frac{N}{t_{ind}} \tag{9}$$

By combining eqs 6−9 at maximum supersaturation where $C^* = C_{met}^*$ (C_{met}^* is the equilibrium concentration at the metastable limit), it is possible to estimate φ_{het}, b and f.

Method 3. The aforementioned two approaches use several assumptions, which can significantly affect the accuracy of the kinetic parameters obtained. The following approach avoids these assumptions by applying a simplified but generic dynamic model for the crystallization process to estimate the kinetic parameters.

The crystallization process is described by the population balance equation (PBE).[31] The solution of the PBE provides the complete CSD, $f_n(L, t)$. A computationally efficient method to solve for the PBE is to use the moment transformation, which computes the average and total properties of the solid phase.[31] The jth moment, when only one characteristic size is considered, is defined by

$$\mu_j = \int_0^\infty L^j f_n(L, t)dL \tag{10}$$

where $f_n(L, t)$ is the crystal size distribution, t is the time, and L is the crystal size. Hence, it is possible to obtain a complete,

yet simple, model for the crystallization process by considering the first four moment equations and the mass balance equation,

$$\begin{bmatrix} \dot{\mu}_0 \\ \dot{\mu}_1 \\ \dot{\mu}_2 \\ \dot{\mu}_3 \\ \dot{C} \end{bmatrix} = \begin{bmatrix} B \\ G\mu_0 + Br_0 \\ 2G\mu_1 + Br_0^2 \\ 3G\mu_2 + Br_0^3 \\ -\rho_c k_v (3G\mu_2 + Br_0^3) \end{bmatrix} \tag{11}$$

where C is the solution concentration expressed in mass of crystal per unit mass of solvent, and r_0 is the crystal size at nucleation. B and G are the primary nucleation and growth rates respectively, which are described by power-law kinetics

$$G = k_g \Delta C^g \tag{12}$$

$$B = k_b \Delta C^b \tag{13}$$

where B is the same nucleation rate as in eq 1 defined on a number basis.

For unseeded systems, the initial condition for eq 11 is given by $\mu_i(0) = 0$ ($i = 0, 1, 2, 3$), and $C(0) = C_i$. The size of the nuclei is considered negligible ($r_0 \simeq 0$). The consideration of primary nucleation as the dominant form of nucleation is valid from $t = 0$ to a short period after t_{ind}, where the surface area of the crystals are not large enough for substantial secondary nucleation to occur.

To estimate the four kinetic parameters (k_b, b, k_g, g), the experimental data are fitted to the output of the model (concentration C and moment ratios μ_1/μ_0, μ_2/μ_0, and μ_3/μ_0) by the nonlinear least-squares technique. The experimental data used includes the measurements from the ATR-FTIR and focused beam reflectance measurement (FBRM) during a short period after t_{ind}.

The estimation of the model parameters requires the solution of a nonconvex, nonlinear programming problem, which was solved using a sequential approach. In this approach, the objective function is calculated in the discrete time points $t_{0,l} < t_{1,l} < ... < t_{K_l}$ with $l = 1, ..., N_{ex}$ (N_{ex} being the number of experiments) and K_l the number of discrete time points in experiment l, and the estimation problem is formulated as

$$\min_{\theta} \{J_{est} = \sum_{l=1}^{N_{ex}} \sum_{k=0}^{K_l} \sum_{i=1}^{N_y} \{(y_i(t_{k,l}; \theta) - y_i^{exp}(t_{k,l}))^2\} \tag{14}$$

subject to model equations (11) and

$$\theta_{min} \le \theta \le \theta_{max} \tag{15}$$

where N_y is the number of measured model outputs (y), y_i^{exp} are the experimental values, θ is the model parameter vector with N_θ elements and bounds θ_{min} and θ_{max}, respectively. In the case of Method 3, $y = [C, \mu_1/\mu_0, \mu_2/\mu_0, \mu_3/\mu_0]$ and $\theta = [k_b, b, k_g, g]$ were used. To evaluate the robustness of the identified model, the confidence intervals of the estimated parameters were calculated. The measurement matrix is given by the block matrix

$$M_\theta = \begin{bmatrix} M_\theta^0 \\ M_\theta^1 \\ \vdots \\ M_\theta^{k_{N_{ex}}} \end{bmatrix} \tag{16}$$

with $k_{N_{ex}} = \sum_{l=1}^{N_{ex}} K_l$ number of ($N_y \times N_\theta$) sensitivity matrixes,

$$M_\theta^{k_l} = \frac{dy^{k_l}}{d\theta} \tag{17}$$

with $k_l = 0, ..., K_l$. The precision matrix (P), covariance matrix (V) are given by

$$P = (M_\theta^T M_\theta)^{-1} \tag{18}$$

$$V = s_R^2 P \tag{19}$$

where the residual variance (assuming that it is equal to the measurement variance) is given by $s_R^2 = J_{est}/N_{df}$, with $N_{df} = N_y(k_{N_{ex}} + 1) - N_\theta - 1$ being the number of degrees of freedom. The confidence intervals are calculated using the t-test,[32]

$$\theta = \hat{\theta} \pm t_{\alpha/2,N_{df}} \sqrt{diag(V)} \tag{20}$$

where $\hat{\theta}$ is the nominal parameter vector, and $t_{\alpha/2,N_{df}}$ is the t distribution with N_{df} degrees of freedom. The 95% confidence intervals are obtained for $\alpha = 0.05$. For Methods 1 and 2, the confidence intervals were calculated applying a similar approach, but using the corresponding model outputs and measurements at a single time step (induction time) in each experiment.

3. Experimental and Theoretical Assessment of the Approaches

The model system studied is the cooling crystallization of paracetamol (PCM) from water. The solubility of paracetamol in water (g PCM/g water) as a function of temperature (in K) is given by,[28]

$$C^*(T) = 1.5846 \times 10^{-5} T^2 - 9.0567 \times 10^{-3} T + 1.3066 \tag{21}$$

Paracetamol (4-acetamidophenol, Aldrich) and degassed, deionized water were used to prepare the solutions, and the experiments were conducted in a 500 mL jacketed round-bottom flask. The solution was agitated by a magnetic stirrer. The Lasentec FBRM was used to detect the metastable limit[28] and to measure the chord length distribution (CLD) of the solid phase, which was used to estimate the particle size distribution. The in situ solution concentration was measured using ATR-FTIR spectroscopy as described previously.[28] For comparison, the nucleation points were also detected using the ATR-FTIR data (change in concentration) as well as by the naked eye (cloud formation). Two series of metastable zone experiments were carried out. The first batch consists of five sets of experimental data (S1−S5) obtained at slow cooling rates in the range 3.22−4.03 °C/h using different initial paracetamol concentrations. The second series of data contains 17 sets of experiments (F1−F17) performed at a constant fast cooling rate of 30 °C/h (0.5 °C/min) using different initial concentrations. Figure 1 illustrates the metastable zones (MSZ) for the two set of experiments. As expected, for the fast cooling rates the metastable zone width is larger than that for the slow cooling rates. For the slow cooling rates, the cloud points detected by the FBRM, ATR-FTIR, and naked eye are also shown in Figure 1. All three detection methods indicated very similar metastable zone widths, therefore for the sake of simplicity, for fast cooling rates only the cloud points detected by the FBRM are presented. The MSZ corresponding to the fast cooling rates also shows larger uncertainties. Table 1 shows the experimental conditions, the obtained metastable zone widths (in terms of maximum undercooling,

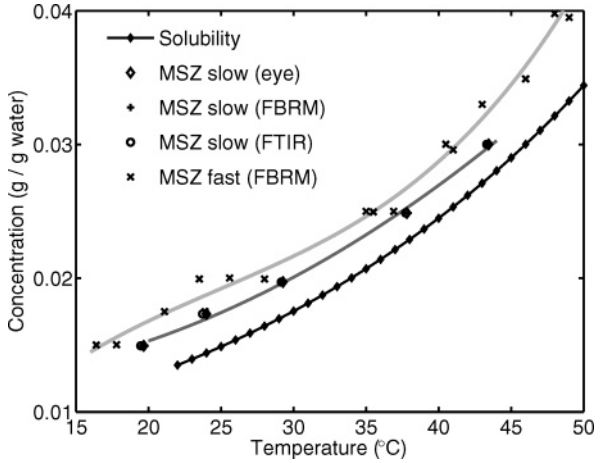

Figure 1. Experimental solubility curve and metastable zone limits for paracetamol in water detected by FBRM, ATR-FTIR, and the naked eye. The dark- and light-gray lines are the trend lines (second and third order polynomials fitted to the experimental points) that show the metastable limits for the slow and fast cooling rates, respectively.

Table 1. Experimental Conditions and Measured Data

exp.	β (°C/h)	C_i (g/g water)	ΔT_{max} (°C)	L_d (μm)
S1	3.8	0.030	2.3	9.5
S2	3.4	0.015	5.3	18.4
S3	3.2	0.020	4.6	16.5
S4	4.0	0.018	6.6	17.4
S5	3.9	0.025	3.3	10.0
F1	30.0	0.020	10.7	9.7
F2	30.0	0.017	9.2	7.5
F3	30.0	0.015	8.6	7.8
F4	30.0	0.014	8.7	6.9

ΔT_{max}), and average particle sizes (L_d) at the induction time t_{ind}, for the first set of experiments and for selected experiments from the second set. The data presented in Table 1 also show the effect of the cooling rate on the size of nuclei (L_d). Crystals are significantly smaller overall for the fast cooling rates than for the slow ones. This is in correlation with the nucleation theory and practical observations that indicate that applying very fast cooling rates can result in a large number of small nuclei due to the higher supersaturation at which the critical cluster forms.[33] The data from experiments F1−F4 are used to test the models obtained and are excluded from the parameter estimation.

The parameters estimated from the three methods are summarized in Table 2, and the predicted metastable zone widths are presented in Tables 3 and 4. The following analyzes evaluate the accuracy of the parameters estimated from the three different approaches.

Method 1. When only experimental data for slow cooling rates (S1−S5) are used to estimate the parameters with this method (part a of Method 1), the model obtained is unable to predict the experimental data for the fast cooling. The average absolute relative error obtained is more than 165% (Table 4). Using the additional data from the fast cooling experiments (F5−F17) significantly improves the quality of the prediction (Table 4, part b of Method 1), but the confidence intervals of the parameters are still large (Table 2). This is not surprising because metastable zone widths for various cooling rates are required to estimate the nucleation parameters using Method 1.

Method 2. This method leads to large errors in predicting the metastable zone widths for both slow and fast cooling rates (Tables 3 and 4) from the experimental data used. On the basis of the variance of repeated experiments, errors around 50% are expected. Hence, such large errors are not unacceptable. The large confidence interval obtained when estimating both parameters $\ln[(b+1)\varphi_{het}]$ and f (part a of Method 2) indicates that the reliability of the parameters is low. As the different parameters are sensitive to different ranges of experimental conditions, it is not possible to simultaneously estimate both parameters using the same set of experimental data (S1−S5). On the basis of the confidence interval shown in Table 2, the sensitivity of the parameter $\ln[(b+1)\varphi_{het}]$ is much smaller than that of f. Hence, the parameter f is estimated again (part b of Method 2) by considering that $b = 6.23$ (from Method 3) and $\varphi_{het} \simeq 10^{-11}$.[13,33] A significantly smaller confidence interval for f is obtained, but there was no reduction in the error for the predicted metastable zone widths. The small reduction factor f, obtained in both cases, indicates that the nuclei have a strong affinity (small contact angle) to the surface of foreign particles present in the system.[13,34]

Method 3. This method gives the nucleation parameters within acceptable confidence intervals, and provides a good estimate of the growth kinetics (Table 2), which are in good correlation with data reported in the literature.[35] Moreover, all of the parameter values obtained with this approach are physically realistic. The obtained model is able to estimate reasonably well the metastable zone width and average crystal size at the induction time for most of the experiments (Tables 3 and 4).

Figure 2 shows the experimental data and the model prediction for experiment S5. A reasonable fit around the metastable zone can be observed. The difference between the model prediction and the experimental data increases with time, which is partly caused by the error from the estimation of the moments of the CSD from the experimental CLD. In this approach, the CSD is obtained from the CLD by considering spherical crystals. Microscopic analysis revealed that the crystals at induction time are hexagonal, which were approximated as spheres, within acceptable errors. However, the aspect ratio of the shape of the crystals changes as they grow. Thus, the CSD estimated based on equivalent diameters can be significantly different from the actual CSD. Different nucleation mechanisms (e.g., secondary nucleation) could also come into effect in the experiments, increasing the uncertainty in the identified model.

Figure 3 shows the simulated nucleation and growth rates obtained using the conditions of experiment S5. The nucleation rate is very small for a long period of time after the supersatu-

Table 2. Results of the Parameter Estimation Using Different Approaches (95% Confidence Level)

method	b	$\ln(k_b)$	g	$-\ln(k_g)$
Method 1a (based on experiments S1−S5)	1.29 ± 2.73	6.49 ± 16.90	-	-
Method 1b (based on all experiments except F1−F4)	2.71 ± 1.74	2.81 ± 2.80	-	-
Method 2a (estimating 2 param. based on S1−S5)	$f = 0.0070 \pm 0.0350$	$\ln[(b+1)\varphi_{het}] = -16.03 \pm 208.9$	-	-
Method 2b (estimating f from $\varphi_{het}=10^{-11}$; b=6.23; S1−S5)	$f = 0.0054 \pm 0.0034$	-	-	-
Method 3 (based on S1−S5)	6.23 ± 0.93	45.81 ± 4.55	1.54 ± 0.48	4.11 ± 1.23

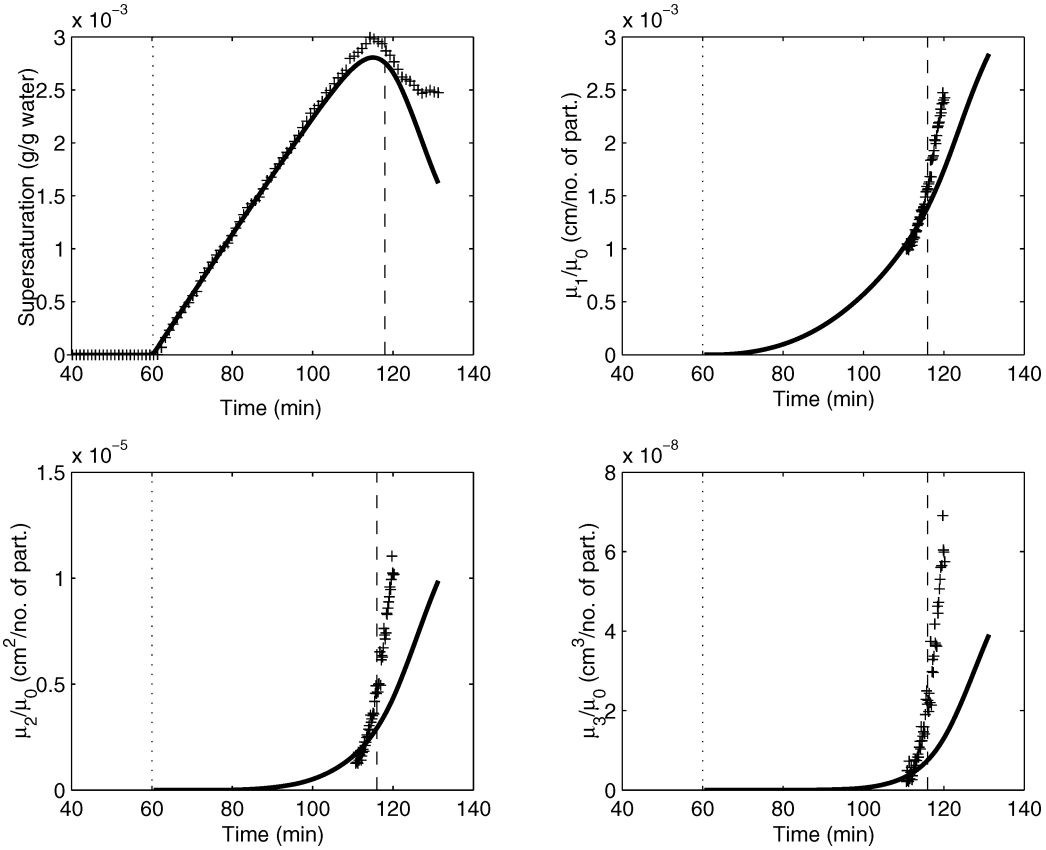

Figure 2. Comparison between experimental data S5 (+) and simulation results (solid line) using the model identified with Method 3. Dotted vertical line indicates generation of supersaturated state; dashed vertical line indicates the time up to which experimental data is used in the parameter estimation.

Table 3. Prediction of Maximum Undercooling and Average Particle Size for the Data Used in the Parameter Estimation

	Method 1a	Method 1b	Method 2a	Method 2b	Method 3	
experiment	ΔT_{max} (°C)	ΔT_{max} (°C)	ΔT_{max} (°C)	ΔT_{max} (°C)	ΔT_{max} (°C)	L_d (μm)
S1	3.7	2.2	3.3	3.3	3.2	12.6
S2	5.2	5.7	7.5	7.5	7.2	17.5
S3	3.7	3.1	4.1	4.1	4.5	14.5
S4	4.3	4.1	4.6	4.6	5.1	15.3
S5	4.0	2.6	3.5	3.5	3.3	10.5
avg. abs. rel. error	29.2%	19.7%	26.3%	26.4%	20.0%	13.3%

Table 4. Prediction of Maximum Undercooling and Average Particle Size for Unforeseen Data

	Method 1a	Method 1b	Method 2a	Method 2b	Method 3	
experiment	ΔT_{max} (°C)	ΔT_{max} (°C)	ΔT_{max} (°C)	ΔT_{max} (°C)	ΔT_{max} (°C)	L_d (μm)
F1	22.9	9.3	4.2	4.2	8.3	8.6
F2	24.2	10.9	4.9	4.9	10.0	9.3
F3	29.1	18.1	7.7	7.8	12.2	7.3
F4	22.0	8.3	4.1	4.2	8.4	8.6
avg. abs. rel. error	165.9%	36.3%	42.8%	42.3%	18.8%	16.6%

rated state is generated. After a certain supersaturation is reached, the nucleation rate rapidly increases to its maximum value at the maximum supersaturation, after which it decreases steeply. The growth rate presents a more gradual variation with supersaturation.

Because the model used in Method 3 is general and is capable of predicting the experimental observations reasonably well, it is used as a theoretical assessment of the first two approaches.

Theoretical Assessment of the Methods. Figure 4 shows the linear dependence of $\ln(\beta)$ on $\ln(\Delta T_{max})$ from experiments S1−S5, simulated using the model obtained by Method 3. The slopes of the lines (m) are approximately equal, and average about 3.3, similar to the value of b (= 2.71) obtained from part b of Method 1. The model from Method 3 gives an apparent nucleation order similar to the apparent nucleation order obtained from Method 1. Method 1 is based on the assumption that the onset of nucleation happens when the event is detected at the induction time (t_{ind}) with nuclei forming at their detectable size (L_d). Equation 5 is derived on the basis of this assumption. However, it is more correct to assume that nuclei are formed at their critical size $r_0 \rightarrow 0$ during the period $0 \leq t \leq t_{ind}$, and then they grow in the remaining time interval ($t_{ind} - t$) to a detectable size L_d with growth kinetics described by eq 12.[18]

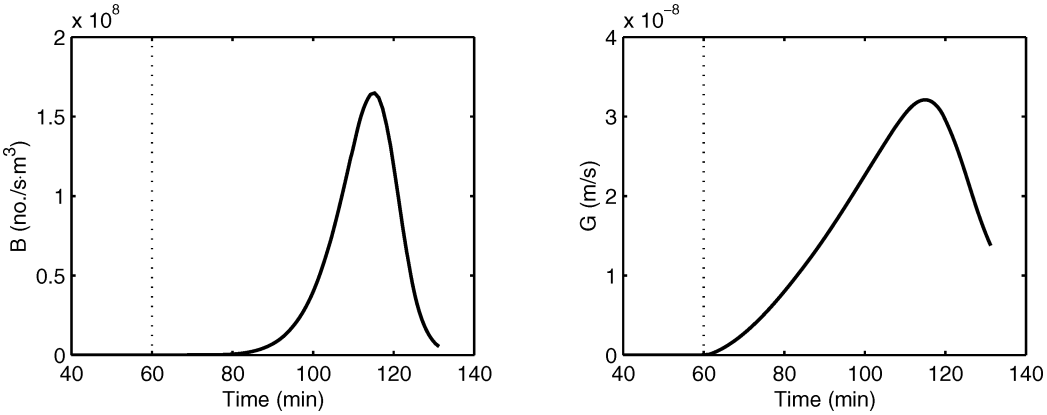

Figure 3. Simulated nuncleation rate (left) and growth rate (right) corresponding to experiment S5.

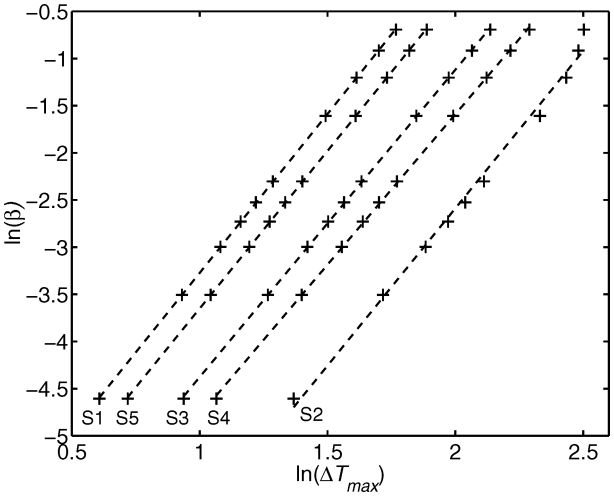

Figure 4. Results of the simulated experiments using the initial concentrations from experiments S1−S5 (+ = simulation results, dashed line = best linear fit).

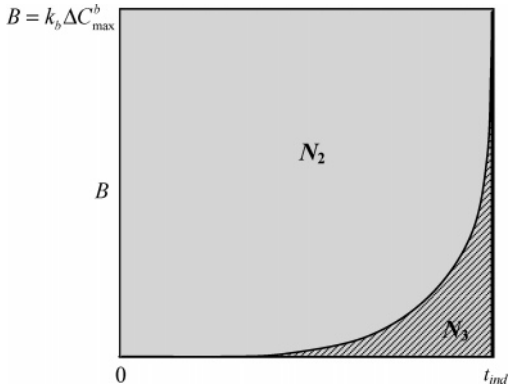

Figure 5. Area representing the number of nuclei estimated by Method 2 (N_2) and Method 3 (N_3).

In this case, a similar expression to (5) can be derived (see Appendix),

$$\ln(\beta) = (m - 1)\ln\left(\frac{dC^*}{dT}\right) + \ln(K) + m\ln(\Delta T_{\max}) \quad (22)$$

where the significance of the slope and intercept are inherently different. From the resulting expression for m (see Appendix), the nucleation order can then be written as

$$b = 4m - 3g - 4 \quad (23)$$

Fitting the simulated data in Figure 4 to eq 22 gives $b \simeq 4.6$ and $k_b \simeq 38$, which are closer to the input values of the simulations. However, the exact values of the input parameters are not recovered because a constant value of dC^*/dT is assumed in the derivation of (22). In fact, for the conditions simulated, dC^*/dT increases by 25−45% of the initial values during $0 \le t \le t_{ind}$, which results in the discrepancies observed.

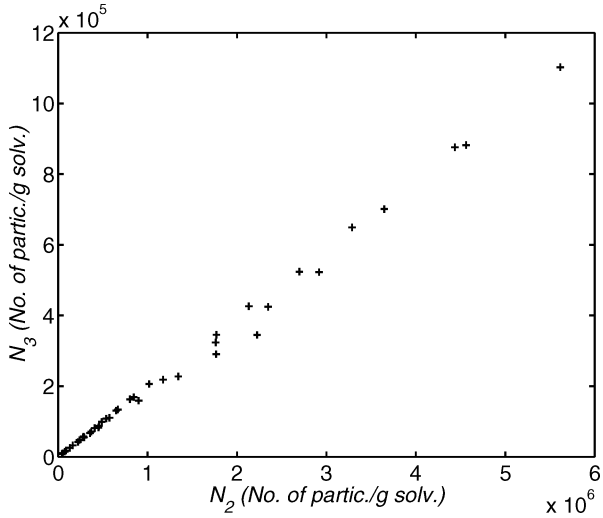

Figure 6. Comparison between the simulated number of particles using Methods 2 and 3 corresponding to different cooling rates and initial concentrations.

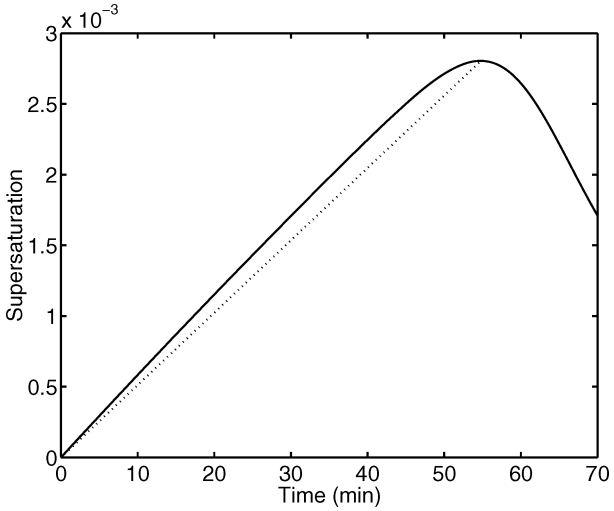

Figure 7. Variation of supersaturation corresponding to the simulated experiment S5, (solid line = integration of the moment model, dotted line = considering constant dC^*/dT).

In Method 2, eq 8 is derived using the nucleation rate expression based on maximum supersaturation for the entire interval $0 \le t \le t_{ind}$, which overestimates the number of nuclei generated during this period. As can be seen in Figure 3, the nucleation rate varies significantly from the creation of supersaturation until the maximum supersaturation is reached. Assuming a constant dC^*/dT for $0 \le t \le t_{ind}$, it can be easily shown that the number of nuclei obtained by Method 2 (N_2) and Method 3 (N_3) is related by

$$\frac{N_2}{N_3} = \frac{\int_0^{t_{ind}} k_b \Delta C_{max}^b dt}{\int_0^{t_{ind}} k_b \Delta C^b dt} \simeq b + 1 \tag{24}$$

Figure 5 depicts the overestimation of the number of nuclei formed. The linear dependence between N_2 and N_3 for different operating conditions (using parameters estimated by Method 3) is illustrated in Figure 6 with N_2/N_3 ranging from 4.9 to 6.4. The ratios are smaller than the suggested value ($b + 1 = 7.23$) because of the error introduced by assuming constant dC^*/dT. This is further substantiated by Figure 7, which shows the variation of the supersaturation with time based on the solubility curve and the assumption of a constant dC^*/dT. As the actual supersaturation is higher, more nuclei are generated (larger N_3) and the actual values of N_2/N_3 are smaller than that approximated by eq 24. The error due to the assumption of a constant dC^*/dT depends on the cooling rate and the initial concentration, causing the slight dependence of the calculated ratios on these parameters.

4. Conclusions

The model parameters for the crystallization of paracetamol from water were determined by applying parameter estimation to data obtained from metastable zone width experiments. This method is based on a simplified by generic dynamic model of the crystallization process, which describes the solid phase and solution concentration without making simplifying assumptions used in previous approaches. The kinetic parameters are estimated by fitting the output of the model to information provided by concentration and particle size distribution measurements using ATR-FTIR spectroscopy and laser backscattering (FBRM). The model obtained with this method captured very well the experimental observations. A detailed theoretical analysis of the previous methods, based on the model derived by the proposed procedure, demonstrates the extent to which errors are introduced by the assumptions used in these approaches. The difference in parameter values obtained between the current method and the previous methods is consistent with the assumptions used in the previous approaches.

Appendix

Assuming that nuclei are formed at their critical size $r_0 \to 0$ during the period $0 \le t \le t_{ind}$ and then they grow in the remaining time interval ($t_{ind} - t$) to a detectable size L_d with growth kinetics described by eq 12, then eq 22 can be derived as follows:

The supersaturation in the period $0 \le t \le t_{ind}$ is expressed by a relation similar to eq 7

$$\Delta C = \frac{dC^*}{dT} \beta t \tag{A1}$$

Nuclei of size $r_0 \to 0$ formed during $0 \le t \le t_{ind}$ grow in the remaining time interval ($t_{ind} - t$) to a detectable size L_d with growth kinetics described by eq 12,

$$L_d = \int_t^{t_{ind}} k_g \Delta C^g = \int_t^{t_{ind}} k_g \left(\frac{dC^*}{dT} \beta t\right)^g = \frac{k_g}{g+1} \left(\frac{dC^*}{dT} \beta\right)^g (t_{ind}^{g+1} - t^{g+1}) \tag{A2}$$

Using nucleation kinetics given by eq 13, the overall mass of the crystals formed at t_{ind} is

$$m_c = \int_0^{t_{ind}} L_d^3 k_v \rho_c \frac{dN}{dt} dt = \int_0^{t_{ind}} L_d^3 k_v \rho_c k_b \Delta C^b dt \tag{A3}$$

Substituting eqs 7, A1, and A2 into A3, the evaluation of the integral results in

$$m_c = \frac{k_v \rho_c k_b k_g^3}{(g+1)^3} q \left(\frac{dC^*}{dT} \beta\right)^{3g+b} \left(\frac{\Delta T_{max}}{\beta}\right)^{3g+b+4} \tag{A4}$$

where $q = 1/(b + 1) - 3/(g + b + 2) + 3/(2g + b + 3) - 1/(3g + b + 4)$.

Defining

$$K = \left(\frac{k_v \rho_c k_b k_g^3}{m_c (g+1)^3} q\right)^{1/4} \tag{A5}$$

and $m = (3g + b + 4)/4$, eq A4 can be written as follows

$$\ln(\beta) = (m-1) \ln\left(\frac{dC^*}{dT}\right) + \ln(K) + m \ln(\Delta T_{max}) \tag{A6}$$

which gives eq 22.

List of Notation

B = primary number nucleation rate
B_m = primary mass nucleation rate
b = kinetic parameter (exponent) for nucleation
C = solute concentration
C^* = equilibrium concentration of solute
C_c = molar density of crystal
C_{max} = maximum solute concentration
C_{met}^* = equilibrium concentration at the metastable limit
D_{AB} = diffusion coefficient
f = reduction factor
$f_n(L, t)$ = number population density function
G = growth rate
g = kinetic parameter (exponent) for growth
J_{est} = estimation objective function (sum square error)
K_l = number of discrete time points (where measurements were taken) in experiment l
k_b = kinetic constant for number nucleation rate
k_b' = kinetic constant for mass nucleation rate
k_g = kinetic constant for growth rate
k_v = volumetric shape factor
L = characteristic crystal size
L_d = size of detectable nucleus
M_θ = measurement block matrix
$M_\theta^{k_l}$ = parameter sensitivity matrix corresponding to discrete time point and experiment k_l
m = apparent nucleation order obtained from method 1
N_2 = number of nuclei formed in the time period $t \in (0, t_{ind})$ calculated with method 2

N_3 = number of nuclei formed in the time period $t \in (0, t_{ind})$ calculated with method 3
N_A = Avogadro number
N_{df} = number of degrees of freedom
N_{ex} = number of experiments
N_y = number of measured model outputs
N_θ = number of model parameters
P = precision matrix
r_0 = crystal size at nucleation
S = supersaturation ratio
s_R^2 = residual variance
T = temperature
T_s = equilibrium (saturation) temperature
t = time
t_{ind} = induction time (time from the generation of supersaturated state until the particles become of detectable size, L_d
$t_{\alpha/2,N_{df}}$ = t distribution with N_{df} degrees of freedom
V = covariance matrix
y = model output vector
y_i^{exp} = experimental measurement vector

Greek symbols

β = cooling rate
ΔC = supersaturation
ΔC_{max} = maximum supersaturation
ΔT_{max} = maximum undercooling
φ_{het} = heterogeneity factor
$\mu_i = i^{th}$ moment of the crystal size distribution given by $f_n(L, t)$
θ = model parameter vector
$\hat{\theta}$ = nominal parameter vector
θ_{min} = vector of minimum bounds on model parameters
θ_{max} = vector of maximum bounds on model parameters
ρ_c = density of crystal

Acknowledgment

The first author gratefully acknowledges the financial support from the Engineering and Physical Sciences Research Council (EPSRC) U.K. (EP/E022294/1).

Literature Cited

(1) Braatz, R. D. Advanced Control in Crystallization Processes. *Annual Reviews in Control* **2002**, *26*, 87.

(2) Braatz, R. D.; Hasebe, S. Particle Size and Shape Control in Crystallization Processes. In *Sixth International Conference on Chemical Process Control*, AIChE Symposium Series, Rawlings, J. B., Ogunnaike, B. A., Eaton, J. W., Eds.; AIChE Press: New York, 2002, *98*, p 307.

(3) Miller, S. M.; Rawlings, J. B. Model Identification and Control Strategies for Batch Cooling Crystallizers. *AIChE J.* **1994**, *40*, 1312.

(4) Ma, D. L.; Chung, S. H.; Braatz, R. D. Worst-Case Performance Analysis of Optimal Batch Control Trajectories. *AIChE J.* **1999**, *45*, 1469.

(5) Ma, D. L.; Tafti, D. K.; Braatz, R. D. Optimal Control and Simulation of Multidimensional Crystallization Processes. *Comput. Chem. Eng.* **2002**, *26*, 1103.

(6) Nagy, Z. K.; Braatz, R. D. Open-Loop and Closed-Loop Robust Optimal Control of Batch Processes Using Distributional and Worst-Case Analysis. *J. Process Control* **2004**, *14*, 411.

(7) Nagy, Z. K.; Braatz, R. D. Robust Nonlinear Model Predictive Control of Batch Processes. *AIChE J.* **2003**, *49*, 1776.

(8) Rawlings, J. B.; Miller, S. M.; Witkowski, W. R. Model Identification and Control of Solution Crystallization Processes: A Review. *Ind. Eng. Chem. Res.* **1993**, *32*, 1275.

(9) Sarkar, D.; Rohani, S.; Jutan, A. Multi-Objective Optimization of Seeded Batch Crystallization Processes. *Chem. Eng. Sci.* **2006**, *61*, 5282.

(10) Nagy, Z. K.; Braatz, R. D. Worst-Case and Distributional Robustness Analysis of Finite-Time Control Trajectories for Nonlinear Distributed Parameter Systems. *IEEE Transaction on Control Systems Technology* **2003**, *11*, 694.

(11) Fujiwara, M.; Nagy, Z. K.; Chew, J. W.; Braatz, R. D. First-Principles and Direct Design Approaches for the Control of Pharmaceutical Crystallization. *J. Process Control* **2005**, *15*, 493.

(12) Nyvlt, J. Kinetics of Nucleation in Solution. *J. Cryst. Growth* **1968**, 377.

(13) Mersmann, A. Supersaturation and Nucleation. *Chem. Eng. Res. Des.* **1996**, *74*, 812.

(14) Mullin, J. W. *Crystallization*, 3rd ed.; Butterworth-Heinemann: London, 1993.

(15) Kim, K.-J.; Mersmann, A. Estimation of Metastable Zone Width in Different Nucleation Processes. *Chem. Eng. Sci*. **2001**, *56*, 2315.

(16) Barrett, P.; Glennon, B. Characterizing the Metastable Zone Width and Solubility Curve Using Lasentec FBRM and PVM. *Chem. Eng. Res. Des.* **2002**, *80*, 799.

(17) Garside, J.; Mersmann, A.; Nyvlt, J. *Measurement of Crystal Growth and Nucleation Rates*, 2nd ed.; Institution of Chemical Engineers: Rugby, UK, 2002.

(18) Nyvlt, J.; Söhnel, O.; Matuchova, M.; Broul, M. *The Kinetics of Industrial Crystallization*; Elsevier: Amsterdam, 1985.

(19) Gutwald, T.; Mersmann, A. Evaluation of Kinetic Parameters of Crystallization from Batch and Continuous Experiments. *Sep. Technol.* **1994**, *4*, 2.

(20) Monnier, O.; Fevotte, G.; Hoff, C.; Klein, J. P. Model Identification of Batch Cooling Crystallization through Calorimetry and Image Analysis. *Chem. Eng. Sci.* **1997**, *7*, 1125.

(21) Qiu, Y.; Rasmuson, A. C. Estimation of Crystallization Kinetics from Batch Cooling Experiments. *AIChE J.* **1994**, *40*, 799.

(22) Gunawan, R.; Ma, D. L.; Fujiwara, M.; Braatz, R. D. Identification of Kinetic Parameters in a Multidimensional Crystallization Process. *Int. J. Mod. Phys. B* **2002**, *16*, 367.

(23) Shaikh, A. A.; Salman, A. D.; Mcnamara, S.; Littlewood, G.; Ramsay, F.; Hounslow, M. J. In Situ Observation of the Conversion of Sodium Carbonate to Sodium Carbonate Monohydrate in Aqueous Suspension. *Ind. Eng. Chem. Res.* **2005**, *44*, 9921.

(24) Togkalidou, T.; Tung, H.-H.; Sun, Y.; Andrews, A.; Braatz, R. D. Parameter Estimation and Optimization of a Loosely-Bound Aggregating Pharmaceutical Crystallization Using In-Situ Infrared and Laser Backscattering Measurements. *Ind. Eng. Chem. Res.* **2004**, *43*, 6168.

(25) Wang, F.; Berglund, K. A. Monitoring pH Swing Crystallization of Nicotinic Acid by the Use of Attenuated Total Reflection Fourier Transform Infrared Spectrometry. *Ind. Eng. Chem. Res.* **2000**, *39*, 2101.

(26) Togkalidou, T.; Fujiwara, M.; Patel, S.; Braatz, R. D. Solute Concentration Prediction Using Chemometrics and ATR-FTIR Spectroscopy. *J. Cryst. Growth* **2001**, *231*, 534.

(27) Fevotte, G. New Perspectives for the On-Line Monitoring of Pharmaceutical Crystallization Process Using In Situ Infrared Spectroscopy. *Int. J. Pharm.* **2002**, *241*, 263.

(28) Fujiwara, M.; Chow, P. S.; Ma, D. L.; Braatz, R. D. Paracetamol Crystallization Using Laser Backscattering and ATR-FTIR Spectroscopy: Metastability, Agglomeration, and Control. *Cryst. Growth Des.* **2002**, *2*, 363.

(29) Ruf, A.; Worlitschek, J.; Mazzotti, M. Modeling and Experimental Analysis of PSD Measurements through FBRM. *Part. Part. Syst. Charact.* **2000**, *17*, 167.

(30) Tadayyon, A.; Rohani, S. Determination of Particle Size Distribution by Par-Tec100: Modeling and Experimental Results. *Part. Part. Syst. Charact.* **1998**, *15*, 127.

(31) Randolph, A. D.; Larson, M. A. *Theory of Particulate Processes*; Academic Press: San Diego, California, 1988.

(32) Beck, J. V.; Arnold, K. J. *Parameter Estimation in Engineering and Science*; Wiley: New York, 1977.

(33) Shi, B.; Rousseau, R. W. Crystal Properties and Nucleation Kinetics from Aqueous Solutions of Na_2CO_3 and Na_2SO_4. *Ind. Eng. Chem. Res.* **2001**, *40*, 1541.

(34) Mersmann, A.; Bartosch, K. How to Predict the Metastable Zone Width. *J. Cryst. Growth* **1998**, *183*, 240.

(35) Granberg, R. A.; Block, D. G.; Rasmuson, A. C. Crystallization of Paracetamol in Acetone-Water Mixture. *J. Cryst. Growth* **1999**, *198/199*, 1287.

Received for review May 22, 2006
Revised manuscript received October 27, 2007
Accepted November 16, 2007

IE060637C